CHALMERS

Synthesis, preparation and characterisation of materials for metal air battery applications

Master of Science Thesis in Applied Physics

MARTIN BERGMAN

Department of Applied Physics

Division of Condensed Matter Physics

CHALMERS UNIVERSITY OF TECHNOLOGY

Gothenburg, Sweden, 2013

Synthesis, preparation and characterisation of materials for metal air battery applications

Master of Science Thesis in Applied Physics

MARTIN BERGMAN

Department of Applied Physics

Division of Condensed Matter Physics

CHALMERS UNIVERSITY OF TECHNOLOGY

Gothenburg, Sweden, 2013

Synthesis, preparation and characterisation of materials for metal air battery applications

Master of Science Thesis in Applied Physics

MARTIN BERGMAN

Synthesis, preparation and characterisation of materials for metal air battery applications

MARTIN BERGMAN

Department of Applied Physics
Division of Condensed Matter Physics
Chalmers University of Technology

Abstract

Energy is one of the most important commodities today, as we use it in almost every aspect of our lives. The need to be able to store energy has increased dramatically the last couple of decades, and with the emergence of electric vehicles and increased use of intermittent energy sources this need shows no sign of diminishing.

One way of storing energy is the use of batteries. There are many different types of batteries but one type that has started to receive increased attention lately is the metal-air battery, using oxygen from the atmosphere as one of the electrodes, allowing more of the other electrode to take up the space inside the battery and thereby increasing the capacity both per weight and volume. One of the most promising metals for this use is zinc, which is cheap, abundant and environmentally benign. However, there are problems during recharge of zinc-air batteries, most importantly the formation of so called dendrites, which are structures of zinc that can short circuit the battery. In this report, one method to subdue this dendrite formation is investigated.

The idea is that by applying a film over the electrode the zinc deposition will be more even and dendrite formation will not occur. It has earlier been proven that this concept works with a zeolite film, and this report will cover two parts: 1. Investigate how the impedance of the zeolite film depend on its thickness and 2. Investigate if the concept works with either sol-gel or silica gel films. To further increase the efficiency, experiments were made to functionalize the film so that it acted as a molecular sieve to capture the dissolved zinc ions upon release from the electrode so that they stayed in the vicinity of the electrode.

The results show that the impedance does depend on the zeolite layer thickness, and the alternative methods with sol-gel and silica gel are promising and show proof of concept, giving an increase in efficiency. It was also proven through FTIR measurements that the functionalization worked, but a good preparation method is needed in order to make thorough experiments.

Acknowledgements

This Master's Thesis was performed at Monash University in Melbourne Australia, and it would not have been possible to make it without a lot of help from people I would like to thank here.

First and foremost I would like to thank my supervisors Patrik Johansson, who supplied the contact with Monash, and Douglas MacFarlane, who took me in under his wings and provided good pointers throughout the thesis.

In a close second come Matthias Hilder, who provided enormous help both in the lab, with the theory and with kind support during hard times, and Bjorn Winther-Jensen who always took the time to give good pointers and advice.

Further, I would like to thank the people in the group, especially Vanessa, Orawan, Chun, Matt, Rob, Bartek, Ciaran, Santosh, Jenny, Derrick, Gary, Mega, Ted Naoki and Alison for good times and helping hands.

Finally, and most importantly, I would like to thank my family and friends for always being there for me, even though I wasn't always the easiest person to be there for. Without you and the stability you provide I would never have made it this far and words cannot express my gratitude. From the bottom of my heart: Thank you.

List of abbreviations

CP = Chronopotentiometry

EIS = Electrochemical Impedance Spectroscopy

FTIR = Fourier Transform Infrared

mt = metric tons

PC = Polycarbonate

PEIS = Potentio Electrochemical Impedance Spectroscopy

PS = Poly Styrene

PVA = Poly Vinyl Acetate

SCA = Standard Calomel Electrode

TEOS = Tetraethyl Orthosilicate

THF = Tetrahydrofuran

TMOS = Tetramethyl Orthosilicate

TMSPA = 3-(Trimethoxysilyl)-Propylamine

Table of Contents

Prologue: Electrochemical basics

Before we begin it is important to define some terms first. This report is written by a physics student, for physics students, and as battery research is an electrochemical field, there are some new concepts and terms that are used, and these will be brought up below.

Electrochemical systems deal with transport of charge across the interface between chemical phases, for example, between an electronic conductor (an electrode) and an ionic conductor (an electrolyte). By applying a potential, current passes and there is a charge transport via electrons in the electrode and via ions in the electrolyte. By investigating what happens during this charge transport and which factors affect it, information about the system can be deduced. For all the concepts described in the prologue and for further reading on electrochemical basics; Bard and Faulkner's book "Electrochemical Methods, Fundamentals and Applications", is recommended [1].

It is natural to think about events at a single interface, but this is not possible to achieve experimentally. Instead, it is necessary to study the properties of collections of interfaces called electrochemical cells. In this report, the system in question will be two electrodes separated by an electrolyte. The difference in electric potential will be measured between the electrodes, and this cell potential is a measure of the energy available to drive charge externally between the electrodes. Most of the time, one is interested in only one of these reactions, and the electrode at which it occurs is called the working electrode. To focus on it, the other half of the cell is standardized using a reference electrode, so that the potential difference can be set in reference to a known value.

The change in electric potential when crossing from one conducting phase to another usually occurs almost entirely at the interface. The sharpness of the transition implies that a very high electric field exists at the interface, and one effect of the sudden change in potential is the *double layer capacitance*. There will be an electrical double layer on the interface between the electrode and the electrolyte, since there will be ions from the electrolyte on the surface of the electrode. In turn, the charged electrode will be separated from the charged ions. This separation will be very small, on the order of Ångströms, but charged particles separated by an insulator forms a capacitor. On a bare metal immersed in an electrolyte, this capacitance is usually 20-60 µF for every cm^2 of electrode area [2].

When an external potential is applied, and the potential of the electrode is forced away from its value at open-circuit or equilibrium potential, it is called "polarizing" the electrode. A polarized electrode can cause electrochemical reactions to occur on the electrode surface, giving rise to a current. This current is controlled by the kinetics (the rate or speed) of the reactions and the diffusion of reactants both towards and away from the electrode [2].

The energy of the electrons can be increased by driving the electrode to more negative potentials. Eventually they can reach a level high enough that makes it energetically favorable to transfer into vacant electronic states on species in the electrolyte, as seen in

figure 1 below. In that case, a flow of electrons from electrode to solution occurs. This is called a reduction current.
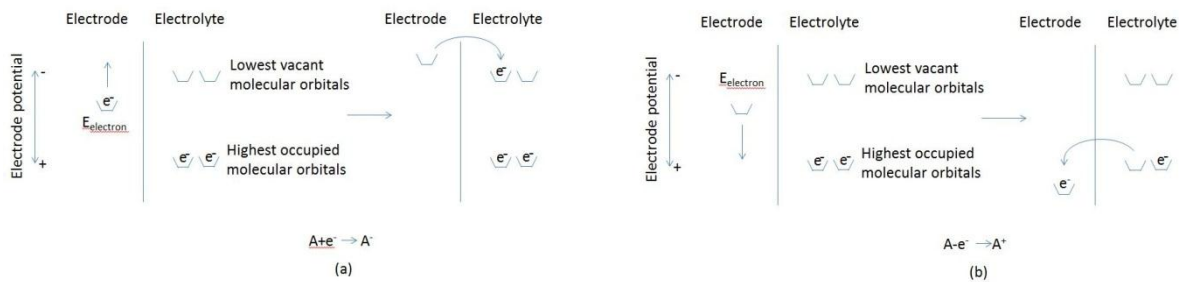
Figure 1: Polarization of the electrode. By driving it to more negative potentials, the energy of the electrons is increased, and can eventually transfer into vacant electronic states on species in the electrolyte. This is called a reduction current (a). By driving it to more positive potentials, electrons on species in the electrolyte can transfer onto the electrode. This is called an oxidation current (b). Illustration inspired by [1].

Similarly, the energy of the electrons can be decreased by driving it to a more positive potential, and eventually the electrons in the electrolyte will find a more favorable energy level on the electrode and will transfer there. Their flow, from solution to electrode, is an *oxidation current*. The critical potentials where oxidation and reduction processes occur are related to the standard potentials, E^0, for the specific chemical substances in the system. However, due to activation energies and other factors, additional potential needs to be applied in order for the flow to occur, and this additional potential required to drive a reaction at a certain rate is called *overpotential*.

The amount of chemical reaction that results from these currents can be calculated with Faraday's law of electrochemistry, which states that:

$$m = \frac{QF}{Mz}$$

where *m* is the mass of the substance deposited or dissolved from the electrode in grams, *Q* is the total electric charge passed through the substance, *F* = 96485 C/mol is the Faraday constant, *M* is the molar mass of the substance and z is the amount of electrons transferred per ion. This means that the amount of chemical reaction caused by the flow of current is proportional to the amount of electricity passed. Since electron transfer causes oxidation or reduction to occur these processes are therefore called *Faradaic processes*.

Electrochemical cells in which faradaic currents are flowing are classified as either *galvanic* or *electrolytic cells*. A *galvanic cell* is one in which reactions occur spontaneously at the electrodes when they are connected externally by a conductor. These cells are often used in conversion of chemical energy into electrical energy. Galvanic cells of commercial importance include *primary (non-rechargeable) cells, secondary (rechargeable) cells,* and *fuel cells*. An *electrolytic cell* is one in which energetically unfavorable electrochemical reactions are forced by applying external energy. These cells are for example used for water splitting for hydrogen production.

1. Introduction

One of the most important commodities today is energy, as we use it in some way in almost every aspect of our lives. The need to store energy is therefore increasing, and batteries are one way to do this. Furthermore, this need is in many different areas. There has been a dramatic increase in portable electronic devices the last couple of decades, with the need of smaller batteries. The emergence of electric and hybrid vehicles contributes a market for medium sized batteries, and the increased use of intermittent energy sources could use large batteries as a way to level the load. A German study showed that a one hour miscalculation on the wind energy forecast creates a need of 5-7 GW. However, today, less than 1% of the grid storage is covered by batteries, mainly for excessive cost reasons [3]. Therefore, there is a big interest in developing batteries. As it is, batteries already comprise a market of several billions of dollars per year worldwide [4], and nothing indicates that the interest in batteries is decreasing.

1.1 Batteries

The history of batteries date back to the year 1800, when Alessandro Volta invented the Voltaic pile. It was comprised of alternating layers of zinc, electrolyte soaked into cardboard or leather, and silver. It was now, for the first time, possible to supply large currents at high potentials for an extended period of time. Back then, there was a lack of understanding of how the pile worked, but it is now known that the zinc was electrochemically oxidized while the native oxide layer on the silver was reduced. The pile could be "recharged" by disassembling it and re-oxidizing the silver by exposing it to air [4], but it was not considered a rechargeable battery. Since these non-rechargeable batteries were the first types of batteries used, they are called primary [5].

However, in 1860 the first truly rechargeable battery was invented by Gaston Planté, who used lead sheet electrodes with a porous separator between them, and sulphuric acid as the electrolyte. This battery produced a potential of 2V, and because of their low cost and ruggedness these lead acid batteries are still in widespread use as of today [4] [6]. In order to charge the battery it was necessary to use primary batteries, and rechargeable batteries are therefore called secondary. Due to the need of primary batteries in order for secondary batteries to work, they did not really generate a lot of interest until Werner von Siemens invented the dynamo [5].

Since the days of Volta and Planté, there have been a lot of different batteries developed, using different types of electrode materials and electrolytes. However, they all work according to the same basic principles, producing electric energy as a result of spontaneous chemical reactions. On the negative electrode, an oxidation reaction takes place, where the negative electrode reactant (e.g. zinc) releases electrons which are led through the external circuit in order to perform work. The negative electrode is then in an oxidized state (e.g. ZnO). At the same time, the positive electrode reactant undergoes a reduction reaction,

receiving the electrons that have gone through the external circuit (e.g. Mn^{+IV} being reduced to Mn^{+III}) [4].

The driving force of these reactions is Gibbs free energy (ΔG), which is the maximum net work obtainable from a chemical reaction [1], and the value of ΔG for different reactions can be retrieved from thermodynamical tables. From ΔG the theoretical specific energy can be found. This is the maximum amount of energy that can be stored in the battery per unit mass assuming that the excess electrolyte and the terminals have negligible mass, and is defined as [4]:

$$Theoretical\ Specific\ Energy = -\Delta G / \sum Mw$$

where ∑Mw is the sum of the molecular weights of the reactants. From this equation it can be seen that the theoretical specific energy is maximized when ΔG has a large negative value and the molecular weights of the reactants are small. The value of ΔG can be made large by using elements that give up electrons readily in the negative electrode, and these elements are found on the left side of the periodic table. In the same way, the positive electrode should be made up by elements that readily accept electrons, and these materials are found on the right side of the periodic table. In order to minimize the molecular weight, elements at the top of the periodic table should be used. These are some basic guidelines when it comes to choosing electrode materials [4]. However, ideal batteries should not only have high energy density, they should also be inexpensive and made from environmentally friendly materials, and these are still only a few examples of an in reality very long list of demands.

1.2 Metal-air batteries

Of the different types of batteries there is one type that shows special promise, namely the metal-air battery. These batteries use the oxygen from the ambient air as active material at one of the electrodes. Since this material does not need to be kept inside the battery, almost the entire space inside the battery can be used for the active material of the other electrode. This means that batteries with air electrodes have higher capacities, both by weight and by volume. However, in order to be able to take advantage of this the other electrode material need to meet certain requirements [7]:

1. Strong reducing power in order to give a high battery potential
2. A large capacity per weight and/or per volume
3. Low cost, abundant resources and environmentally friendly

Promising candidates include lithium, aluminum, zinc and iron. As can be seen in table 1 below, lithium and aluminum tops the chart when it comes to potential and specific energy. However, the very negative electrode potentials cause them to corrode in aqueous solutions, producing hydrogen. Hydrogen evolution is suppressed on metals such as lead,

11

cadmium, indium, mercury and zinc that exhibit intrinsic high overpotentials for hydrogen evolution. Among these metals, zinc has the lowest equivalent weight, the lowest ecological concern and a very attractive cell voltage in conjunction with an oxygen electrode. Furthermore, zinc is a safe material, can be fully recycled and is abundant. In 1994 there was 6 819 000 metric tons (mt) of zinc mined worldwide with 140 000 000 mt in reserves. In 2005, the corresponding numbers were 10 000 000 and 220 000 000 mt [8], where the increased reserve comes from changes in economic and technical conditions, making it viable to extract a bigger part of the zinc resources.

Table 1: Theoretical electrochemical parameters for electrode materials for metal-air batteries, obtained from [8]. The equivalent mass is calculated with respect to the product of discharge (e.g. ZnO rather than Zn; M_{ZnO}=81.38 g/mol, equivalent mass = 81.38/2=40.69 g). Even though Li and Al have the highest potential and theoretical specific energy, they corrode in aqueous solutions, producing hydrogen. Zinc, on the other hand, has high specific energy and potential while having an intrinsically high overpotential for hydrogen production.

Electrode material	Equivalent mass (g)	Metal/O_2 potential (v)	Theoretical specific energy (Wh/kg)
Li	23.94	3.44	3853
Al	25.99	2.78	2869
Zn	40.69	1.67	1100
Fe	44.92	1.27	758
Cd	73.20	1.2	439

In fact, the only metal-air battery systems available worldwide are primary zinc-air batteries. The specific energy of these batteries is 400-450 Wh/kg, which is five times higher than alkaline batteries and twice as high as primary lithium batteries. In order to avoid self-discharge these batteries are delivered with a sticker covering the air access holes, which is removed before use. After the sticker has been removed, the battery should be used continuously since the air access will result in water exchange and carbon dioxide contamination of the electrolyte, causing deterioration of the battery [7].

In order to be able to make a secondary zinc-air battery, a number of different recharging solutions have been proposed, such as electrical, mechanical, or hydraulic recharging. Each system has its own advantages and disadvantages. Hydraulic recharge is when the zinc-air battery is run in fuel cell mode instead, meaning that there will be a continuous supply of reactants to the electrodes. Mechanical recharge is a similar solution, but then it is the zinc anode that is replaced instead [9]. These methods, however, require special replacement and regeneration stations. Electrical recharge, on the other hand is when the zinc-air battery is operated like any other secondary battery, recharging it by running a current through it. This is simple for the user but will require a bifunctional oxygen electrode that is able to both undergo oxidation and reduction [8]. Furthermore, during electrical discharge there is a formation of dendrites, which are tree-like (dendron is Greek for tree) zinc structures that can penetrate the separator and short circuit the battery [9]. In this report, a method to solve the dendrite formation problem during electric recharge will be investigated.

2. Background

When zinc is dissolved and re-deposited onto electrodes there is a problem called dendritic growth. What this means is that the zinc redeposit in tree-like dendrite structures that risk to short circuit the battery. In order to control this, the idea is to use a layer on top of the electrodes that will subdue this dendritic growth and spread the deposition more evenly. It has been proven by Matthias Hilder et al [10] that this can be done by using zeolites. This method will first be investigated further with impedance spectroscopy in order to determine the thickness dependence of the impedance, before alternative methods and materials of surface functionalization based on sol-gel processes and silica gels are investigated. Furthermore, by functionalizing these gels, specific affinity can be added. Thus the matrix can act as a scavenger for the Zn^{2+} discharge product, keeping it in close vicinity to the electrode instead of being flushed out into the electrolyte, making the recharge process much more efficient.

2.1 Zeolites

Zeolites are a group of microporous minerals that was first discovered in 1756 by Swedish mineralogist Axel F Cronstedt. They are composed of a three dimensional network of aluminium, silicon and oxygen atoms, and this network gives rise to a system of channels and cavities that for each zeolite has a specific diameter of 3-12 Ångströms [11].

In these channels and cavities, positive ions (cations) are bound to the negative ion (anion) structure by weak electrostatic forces. The ions are therefore both mobile and exchangeable, giving rise to an ion exchange property that can be used in order to control the zinc ions [11]. It is this property that is used in order to capture the zinc ions that are released during discharge.

2.2 Sol-gels

A sol is a dispersion of colloidal particles in a liquid, where colloids are solid particles with diameters of 1-100 nm. A gel is an interconnected, rigid network with pores smaller than a micrometer and polymeric chains with an average length of over a micrometer [12]. A sol-gel is formed when the colloidal particles in the sol bind to each other, polycondensates, creating a porous network in a liquid [13].

As early as the mid-1800s it was observed that hydrolysis of tetraethyl orthosilicate (TEOS) under acidic conditions yielded SiO_2 in the form of a "glass-like" material. However, back then, it was necessary to have drying times of a year or more in order to avoid fracturing the sol gel into a fine powder, and consequently the technological interest of the substrate was small [12]. From the late 1800s through to the 1920s, the interest in gels increased, and in the 1950s and 1960s the sol-gel method was used to synthesize a large number of novel

ceramic oxide compositions, involving Al, Si, Ti, Zr, etc, that could not be produced through traditional ceramic powder methods. Furthermore, sol-gel processing yields higher purity and homogeneity compared to traditional methods, and also requires a lower processing temperature. Nowadays, drying can be achieved in days rather than years. The problem with the drying was the cracking that occurred due to the shrinkage that take place when pore liquids are removed from the gels. These stresses are fairly small for small cross sections and can be accommodated by the material, but for larger pieces of sol-gel it can become a problem [12]. One way to create sol-gel is through acid catalyzed hydrolysis.

2.2.1 Acid catalyzed hydrolysis

The polycondensation of the sol occurs through acid or base catalyzed hydrolysis. Hydrolysis means the disruption of chemical bonds by addition of water. A catalyst is something that enhances chemical reaction speed without being consumed itself. Therefore, an acid catalyzed hydrolysis is a splitting of chemical bonds catalyzed by acid. In this case, the chemical to hydrolize is TEOS, seen below in figure 2.
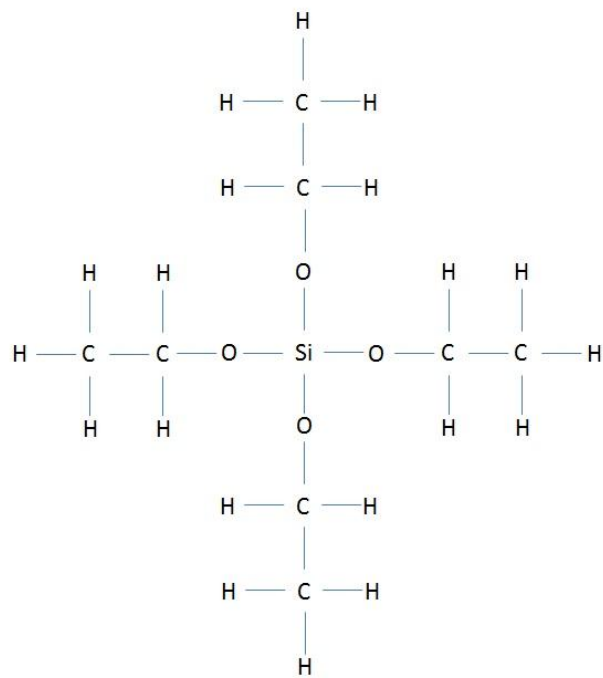

Figure 2: The structure of tetraethyl orthosilicate (TEOS). In the middle is a silicon atom, surrounded by four oxygen atoms, and to each oxygen atom an ethyl group (CH2CH3) is attached.

The atom in the middle is a silicon atom, and the four atoms around it are oxygen atoms. To each oxygen atom an ethyl group (CH_2CH_3, from now on abbreviated Et), is attached. It is sought after to create a network of silicon and oxygen atoms, so the ethyl groups should be hydrolyzed. To focus on one of the ethyl groups, the other arms are named R (to show that they are reacting groups but are not a part of the reaction of interest). The oxygen atom has

two electron pairs not bound, pictured as two lines in figure 3 below. When acid is added the hydrogen ion binds to the oxygen atom and makes the oxygen slightly positive.
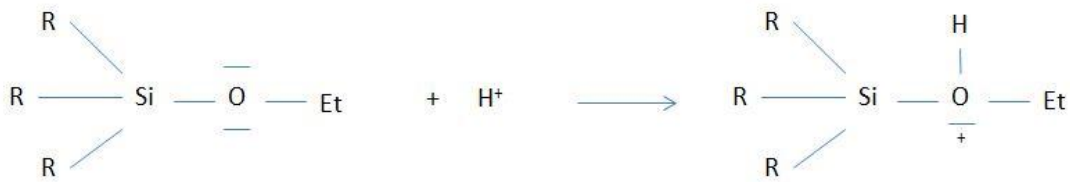

Figure 3: Step 1, the hydrogen atom binds to the oxygen atom

However, oxygen is more electronegative (electronegativity is a measure of how strongly an atom binds electrons to itself) than silicon, so the oxygen steals the electron it previously shared with the silicon in order to neutralize itself. The TEOS then loses a branch, and ethanol (EtOH) is produced, as seen in figure 4.
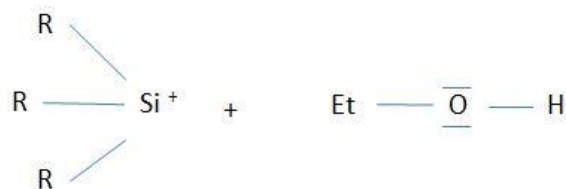

Figure 4: Step 2, the oxygen steals the electron it previously shared with the silicon atom, and ethanol is produced

The silicon that now is positive binds to another TEOS-molecule, as seen in figure 5.
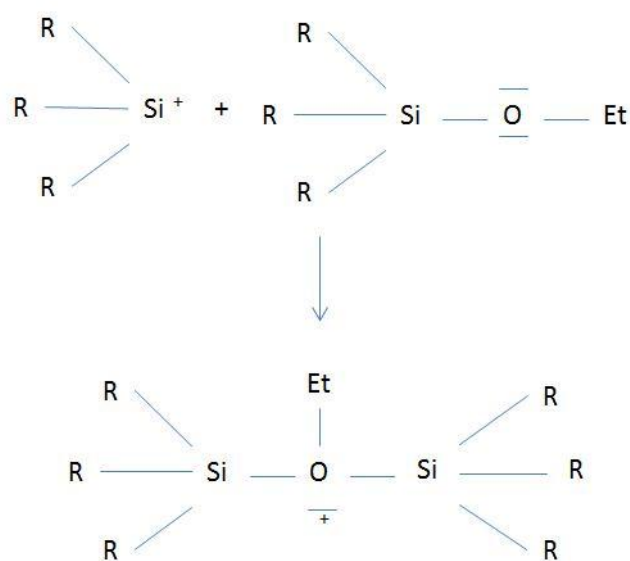

Figure 5: Step 3, the positive silicon binds to an oxygen atom in another TEOS-molecule

15

The oxygen then steals an electron from the ethyl group, and water comes in and pick up the ethyl group, producing more ethanol and a hydrogen ion. The reaction is now self-sustained.
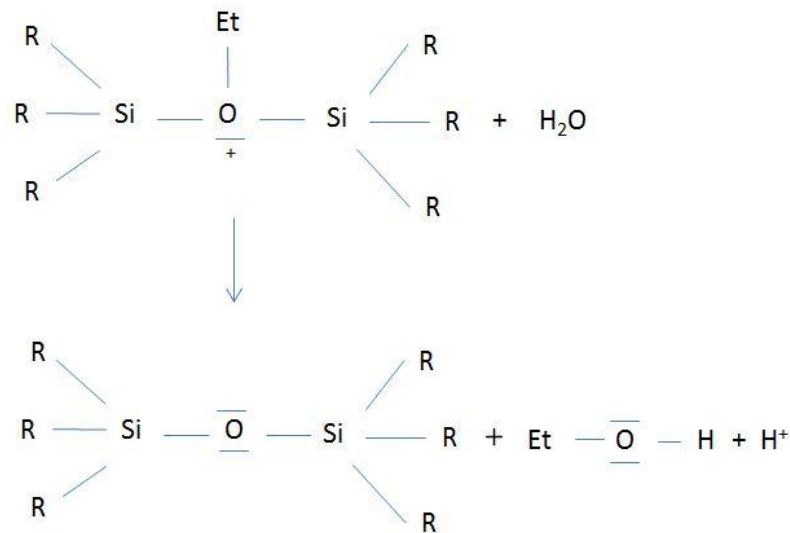

Figure 6: Step 4, the ethyl group is hydrolysed, producing ethanol and another hydrogen ion that can catalyze another reaction, and the network will slowly be built up.

2.3 Silica gels

Silica gel is a network of silica and oxygen, as seen below in figure 7, in powder form. One way to create it is through the sol-gel process described above and then grinding up the sol-gel to a powder [10]. Silica gels are very hygroscopic and is commerisally used for drying of air [14], for example can the small desiccant packages found when purchasing consumer electronics be filled with silica gel.
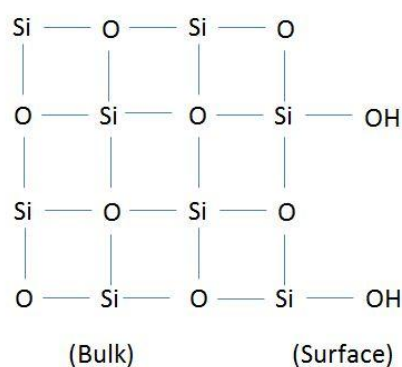

Figure 7: Silica gel network

16

3. Materials preparation

3.1 Zeolites

In order to measure the impedance, titanium electrodes covered with a film of zinc zeolite will be used. This film is produced by mixing powdered zeolite in a solution of tetrahydrofuran (THF) containing 1% polystyrene as a binder, then grind the mix using mortar and pestle, and then pipette it onto the electrode. The reason for the binder was to act as a mechanically stable framework and bind the active material onto the substrate. After drying, the electrodes with the zeolite films on them are laminated, with a 5x5 mm window cut out, so that a set area is used. See figure 8 below.

Figure 8: Titanium electrode with a white zeolite layer in the bottom

The relative amount of the zeolite (or its "thickness") is measured in $\mu g/mm^2$. The electrode is weighed before and after the zeolite film has been applied, so the weight of the amount of zeolite on the electrode is known. The area that the zeolite film covers is then measured, and the thickness will then be the weight divided by the area.

The electrode is then inserted into an electrolyte of either 0.1M $ZnCl_2$ or 0.1M NaCl electrolyte. There were also some measurements made with a lower concentration of $ZnCl_2$, but the conduction was so low that no deposition could take place.

The $ZnCl_2$ was made by dissolving 6.815 g of solid $ZnCl_2$ in half a liter of deionized water (since $ZnCl_2$ has a molar weight of 136.3 g/mol). To make the pH more neutral, the $ZnCl_2$ was heated and diluted sodium hydroxide was added dropwise until precipitate of zinc hydroxide appeared. The solution was then left to cool before filtering out the zinc hydroxide. The pH was then determined to be just over 6 using a calibrated 785 DMP Titrino Merohm pH meter. For the sodium chloride no pH alterations were necessary. It was simply made by dissolving 2.92 g of solid sodium chloride in half a liter of deionized water. Its pH was determined in the same way and had a similar value as the $ZnCl_2$.

3.2 Sol-gels

For the sol-gel approach, three different recipes found in literature were used. First a bulk sol gel recipe [15] that had a molar composition of tetramethyl orthosilicate (TMOS), ethanol, deionized water, and hydrochloric acid of $1:3:5:4.6 \cdot 10^{-4}$. The ethanol is added in order to dissolve the TMOS, since it does not dissolve in water, to produce a homogenous

solution [13]. This mix was then left in a heat bath at 50° C over night for gelling before commencing attempts to dry it and attach it to the electrode.

The other two recipes were of the thin film sol gel type [16], [17]. Recipe [16] used a molar composition of TEOS, ethanol, deionized water and hydrochloric acid of 1:1.5-2.5:2-5:0.01. This mix was then magnetically stirred for 2h before it was applied to the electrode by dip coating, which is an application technique where the electrode is dipped into the solution for ten minutes and then taken out to dry.

Recipe [17] also used dip coating. It had a molar composition of TEOS, deionized water, ethanol and hydrochloric acid of 1:4:5:0.25. This mix was then magnetically stirred for 30 minutes before dip coating the electrode with it. The electrode was then put in a furnace at 110° C for 30 minutes to dry and then heat treated at 500° C for another 30 minutes.

3.3 Silica gels

The silica gel was first functionalized using the chemical 3-trimethoxysilyl-propylamine (TMSPA), seen in figure 9 below.
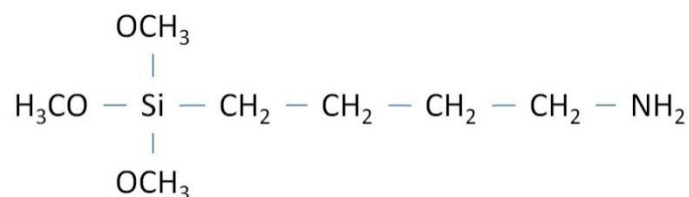

$$H_3CO - \underset{\underset{OCH_3}{|}}{\overset{\overset{OCH_3}{|}}{Si}} - CH_2 - CH_2 - CH_2 - CH_2 - NH_2$$

Figure 9: The molecule 3-(Trimehoxysilyl)-propylamine

The functionalization was made by mixing 1g TMSPA in 50 ml of 90% ethanol and then adding acetic acid until the pH was raised to about 5. Into this mix, 1g of silica gel was inserted, and everything was then stirred overnight before it was filtered, rinsed with ethanol and water and then dried.

The reason for functionalizing the silica gel is the NH_2-group on the TMSPA, called an amine. Amines are derivatives of ammonia (NH_3) where the hydrogen atoms have been replaced by hydrocarbon groups. If one hydrogen atom is replaced it is called a primary amine, two hydrogen atoms replaced makes a secondary amine, and three hydrogen atoms replaced makes a tertiary amine [18]. The reason that the, in this case primary, amine is interesting is that it has a lone electron pair which will bind to the positive zinc ions, forming zinc-amine complexes and thereby keeping the Zn^{2+} close to the electrode.

The activated silica gel was then, like the zeolite, put in a solution of THF including a binder, then mixed with mortar and pestle before it was pipetted onto the electrode and dried. The binders tried were polystyrene (PS), polycarbonate (PC) and polyvinyl acetate (PVA), all with a 1% binder content in the THF.

4. Experimental Techniques

4.1 Electrochemical Impedance Spectroscopy

Electrochemical Impedance Spectroscopy (EIS) is a method that measures the impedance of an electrochemical setup as a function of frequency. There are two different types of systems in electrical circuit theory, namely linear and non-linear, where linear systems have the property of superposition. Impedance analysis of linear circuits is much easier than analysis of non-linear ones, but electrochemical cells are not linear. They can, however, be made pseudo-linear by looking at a sufficiently small element, as can be seen below in figure 10 [2].
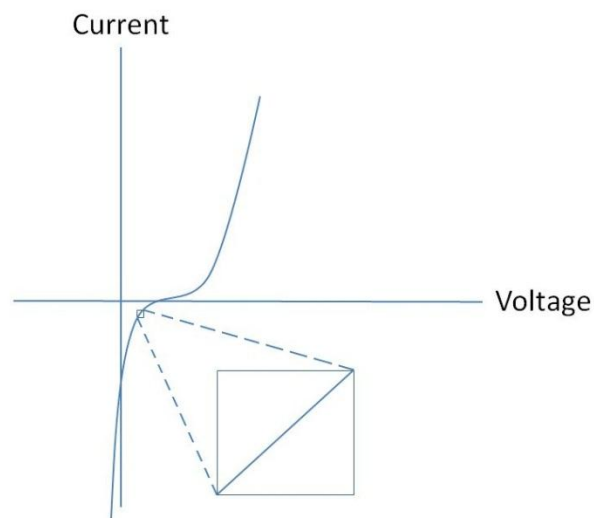

Figure 10: Pseudo-linearity. When looking at a sufficiently small portion of a non-linear curve, that part looks linear [2].

In a potentiostatic electrochemical cell, the potential is the input and the current is the output. By focusing on a small enough portion of the curve, it appears to be linear. In EIS, a small (1 to 10 mV) AC signal is applied to the cell, making the system pseudo-linear. The large non-linear response to the DC potential is not visible because it is only the current at the excitation frequency that is measured [2].

Since the voltage input is known and the current response can be measured, an impedance can be calculated for each frequency with Ohm's law. By taking the real part of the impedance and plot it on the X-axis while taking the imaginary part and plot it on the Y-axis we get a "Nyqvist plot" as seen below in figure 11 [2].
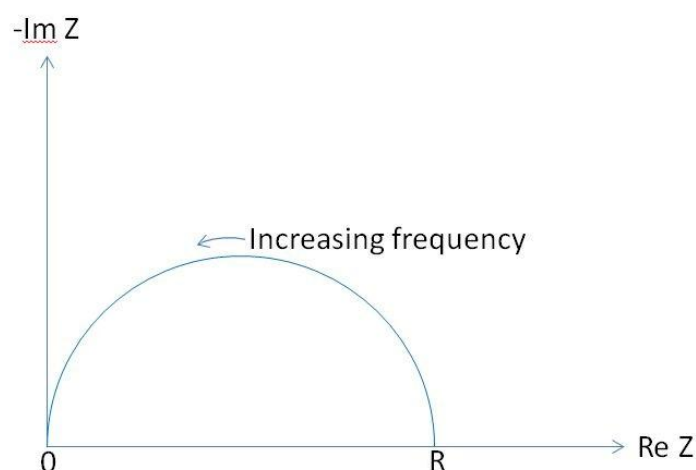
Figure 11: Nyquist plot from EIS measurement.

Notice that the y-axis is negative and that each point corresponds to the impedance at one frequency. The high frequency data is on the left side and the low frequency data is on the right side [2]. These plots often form one or more semicircles as seen in figure 11, and from these semicircles it is possible to find out information about different processes, as will be seen later on.

4.2 Fourier Transform Infrared Spectroscopy

Around 1800, the spectrum of sunlight was studied by Herschel, who used a prism to split up the sunlight and then measured the temperature of each color. He found that the highest temperature was just beyond the red light, in the region we now call infrared. After two centuries of development, it is now possible to use this light to probe molecular vibrations, and this is called infrared spectroscopy [19]. The way it works is that different groups of bonded atoms, different functional groups, vibrate with different energies located in the range of IR radiation and therefore have characteristic infrared absorption bands [19]. This means that if infrared light is sent in, certain frequencies will be absorbed and will show up with lower intensity when the emitted light is analyzed. When the data is converted using Fourier transform, it is known as Fourier Transform Infrared Spectroscopy (FTIR spectroscopy) [20]. With the older techniques, only one resolution element at a time was measured. A survey spectrum is often measured with a resolution of 4 cm^{-1}, so with a spectrum between 400-4000 cm^{-1}, it is only 1/900th of the spectrum that is measured at a time, giving an efficiency of about 0.1%. With the Fourier Transform technique, however, all the resolution elements are measured at the same time. Furthermore, more radiation can be passed between the source and the detector for each element. This means that FTIR will be both faster and more accurate than the older techniques [21].

For a non-linear molecule with N atoms, there are 3N-6 vibrational motions of the molecule atoms, or 3N-6 fundamental vibrations or normal modes. A normal mode of vibration is infrared active (meaning that it absorbs infrared light) if there is a change in the dipole

moment of the molecule during the vibration. This means that symmetric vibrations are usually not detected in infrared, but all asymmetric vibrations of all molecules are detected. Especially for groups with a permanent dipole, strong IR absorptions are observed [19].

The infrared region is divided into three frequency parts (measured in cm^{-1}): far infrared (10 – 400 cm^{-1}), mid-infrared (500 – 4000 cm^{-1}), and near infrared (4000 – 14000 cm^{-1}). FTIR deals with the mid-infrared region, and in this region, two main types of vibrations are observed. These are the stretching vibrations (ν), involving bond-length changes, and bending vibrations (δ), involving changes in bond angles. The stretching vibrations can be modeled with a harmonic oscillator, as can be seen in figure 12 below. Here the atoms are the two weights and the bond is the spring between them, where the spring constant k is the bond strength [19].
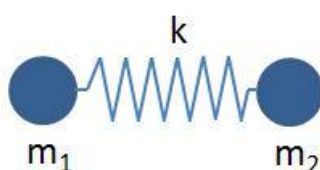

Figure 12: Stretching vibrations modelled with a harmonic oscillator

The vibration frequency ν is given by the equation [19]:

$$\nu = \left(\frac{1}{2\pi c}\right)\sqrt{k(m_1 + m_2)/m_1 m_2}$$

It can be seen that the vibration frequency ν depends on the bond strength (k), with double and triple bonds requiring higher frequency due to stronger bonding (and thereby higher k). This also means that the frequency will depend on the group environment, the electronegativity of neighboring atoms or groups, or hydrogen bonding interactions. If a hydrogen bonding occurs, the bond strength will weaken and shift the frequency peak downwards. It can also be seen that the mass of the atoms involved will affect the frequency, with heavier atoms leading to a downshift [19].

In summary, the frequencies for a given chemical group is expected to show up in specific parts depending on the atoms involved and the bonds between them, and tables are available for the main chemical groups [19].

4.3 Experimental setup

The setup used for the experiments was a so-called three-electrode setup, and can be seen in figure 13 below. The green cable is connected to the specimen (working electrode), the red cable is connected to the counter electrode (which is just a titanium mesh electrode, in order to have a larger area than the working electrode) and the vial in the middle is the reference electrode (a standard calomel electrode, SCE).

Figure 2: Experimental setup for the cycling experiments. The green cable is connected to the working electrode, the red cable is connected to the counter electrode, and the vial in the middle is the SCE reference electrode

4.3.1 Zeolite impedance measurements

In order to see how the thickness of the zeolite layer affects the impedance, the impedance was first measured before any deposition had taken place by using potentio electrochemical impedance spectroscopy (PEIS), which sweep a range of sinuses around a DC potential E. In this case the DC potential was set to 0 and the frequencies swept in this case were 500 kHz - 100 mHz.

The deposition was then performed by running a chronopotentiometry (CP) experiment. This is a technique where the current is controlled, in this case it was set to -400 µA for 8 minutes, and the potential is the variable determined as a function of time. After the deposition, another PEIS measurement was made in order to see the difference in impedance between pre- and post-deposition. After the deposition, however, the frequency 100 mHz. This was because, as will be seen below, there were no interesting phenomena taking place at such low frequencies prior to deposition. PEIS and CP were then alternated for a number of cycles in order to see if there were any long term changes.

4.3.2 Sol-gel and silica gel cycling and efficiency

The cycling of the sol-gel and silica gel was carried out by first applying -50µA for 900 seconds (15 minutes) in order to charge the battery by depositing zinc on the electrode, then running +50µA for as long as possible. This was then repeated for 10 charge-discharge cycles in order to see long term changes. Part of the charging current will be lost to overpotential and side reactions, so the dissolution of zinc during the discharge will not be able to sustain 50µA for 15 minutes. The efficiency is then calculated as the time of dissolution in seconds divided by the 900 seconds of deposition.

5. Results and discussion

In this chapter the results from the experiments laid out in the previous chapter will be presented and discussed. It is divided into three parts according to respective technique, and it will be found that the zeolite thickness indeed does affect the impedance, with thinner layers having less impedance. Furthermore, the sol-gel and silica gels will be found to increase the efficiency as well, but further research needs to be done.

5.1 Zeolites

Measurements for a blank sample and two samples with different zeolite layer thicknesses are shown in the Nyquist plot in figure 14 below. Since the frequency is the highest to the left, the first quarter circle seen between 0 and 15 Ohm on the x-axis corresponds to electron conductivity. This part is mostly due to the electrode and the connections, and since they do not change due to the deposition, there is barely any change in that part between pre-deposition and post-deposition. The semicircle is more interesting as that one is more in the ion conducting region, which is the region that the thickness of the zeolite will affect.

The blue line corresponds to a blank sample, the red line corresponds to a sample with a thin zeolite layer (44 µg/mm^2), and the green line corresponds to a sample with a thicker zeolite layer (131 µg/mm^2). As can be seen, the lines rises upwards in ascending thickness order, with the blue line rising upward first, then the red line and finally the green one. Since no deposition has been made yet, this indicates that the impedance increases with increasing amount of zeolite.

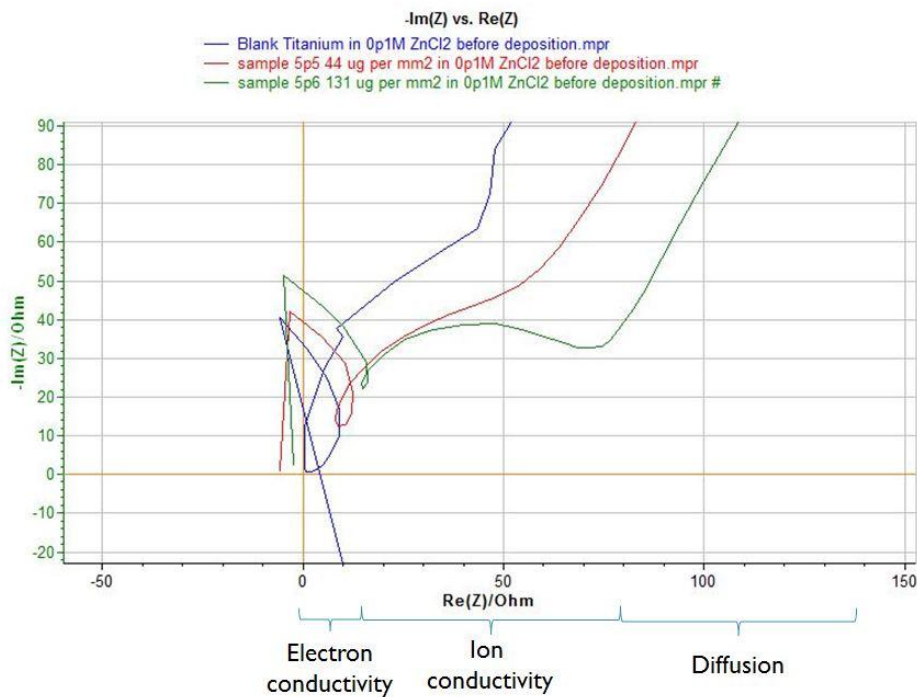**Figure 14: Impedance as a function of thickness of the zeolite layer, prior to zinc deposition, in ZnCl$_2$. As can be seen, the lines rise in ascending thickness order, indicating that the impedance is dependent on the thickness of the zeolite layer.**

This is confirmed in the experiment with NaCl, seen in figure 15 where the blue line, representing the thin sample (41 µg/mm^2) rises upwards before the red line representing the thick sample (127 µg/mm^2). The lack of reference measurement with a blank titanium electrode in the NaCl case is due to the fact that no deposition would be done on a blank electrode in NaCl. There would also be a difference of present ions between the zeolite samples and the blank due to the zinc ions inside the zeolite.
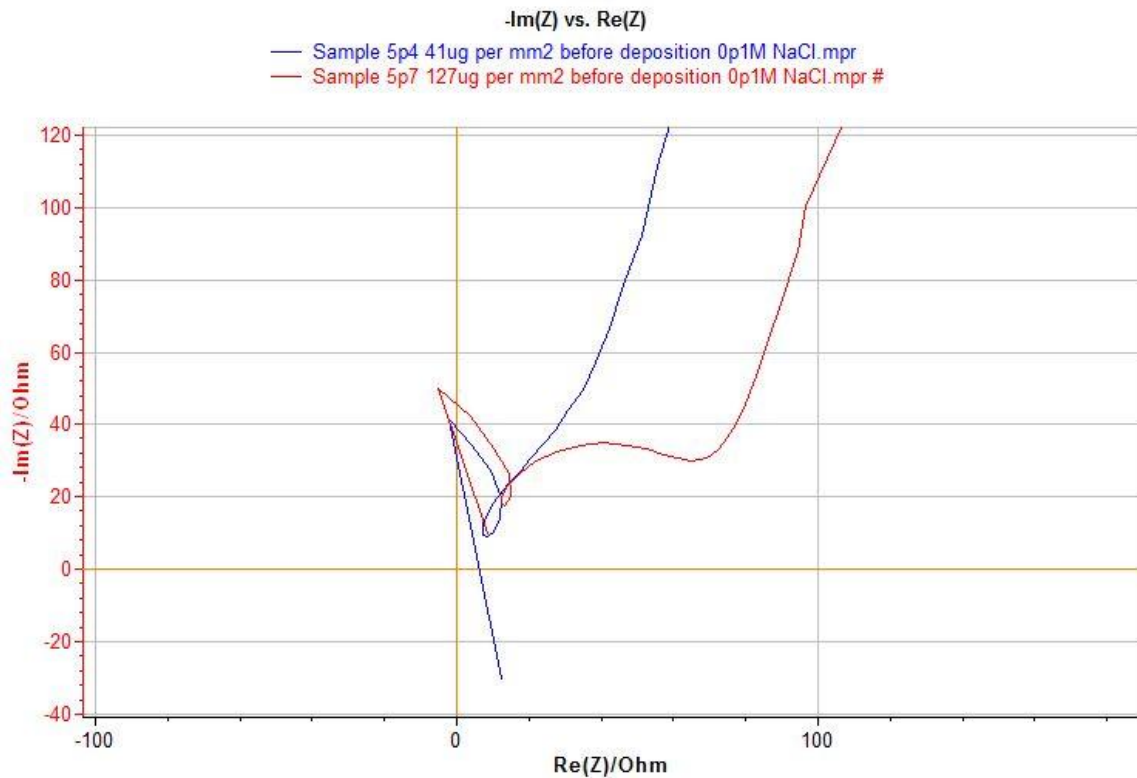

Figure 15: Impedance as a function of thickness of the zeolite layer, prior to zinc deposition, in NaCl. As can be seen, the lines rise in ascending thickness order, indicating that the impedance is dependent on the thickness of the zeolite layer

Impedance measurements after the first deposition can be seen for ZnCl$_2$ in figure 16 and for NaCl in figure 17 below. It can be seen that, after the deposition, the impedance differences due to different thicknesses is still apparent. In the ZnCl$_2$ it is also possible to distinguish between the impedance resulting from the electrolyte (from the blue graph) and how much comes from the zeolite (red and green), respectively. The semicircle of the blank sample (only electrolyte) ends at about 50 ohm, whereas the semicircle for the thin zeolite electrode ends closer to 60 ohm and the semicircle of the thick zeolite ends around 80 ohm. Thus, it is clear by this increase that the impedance increases with zeolite thickness.

However, it is important to notice that if an electrolyte without zinc is used, a thicker zeolite layer will be needed in order to provide more zinc for deposition. Furthermore, regardless which electrolyte is used, a thicker electrolyte will provide more mechanical stability and will facilitate more room for zinc deposition. A case where too much deposition has taken place in relation to zeolite thickness can be seen in figure 18 below, where the dendrite formation can be seen.
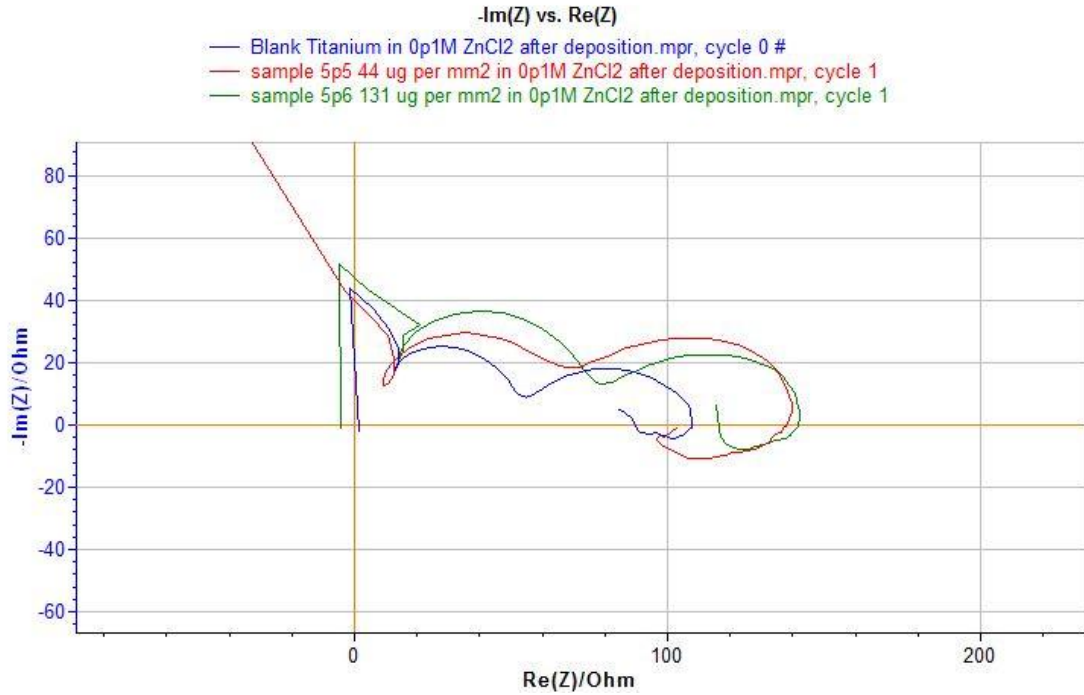
-Im(Z) vs. Re(Z)

— Blank Titanium in 0p1M ZnCl2 after deposition.mpr, cycle 0 #
— sample 5p5 44 ug per mm2 in 0p1M ZnCl2 after deposition.mpr, cycle 1
— sample 5p6 131 ug per mm2 in 0p1M ZnCl2 after deposition.mpr, cycle 1

Figure 16: Impedance measurements after zinc deposition, in ZnCl$_2$. The dependence on thickness can still be seen, but there are also second capacitive semicircles showing up. These are due to a combination of polarization resistance in the electrode and double layer capacitance [22].

-Im(Z) vs. Re(Z)

— Sample 5p4 41ug per mm2 after deposition 0p1M NaCl.mpr, cycle 1
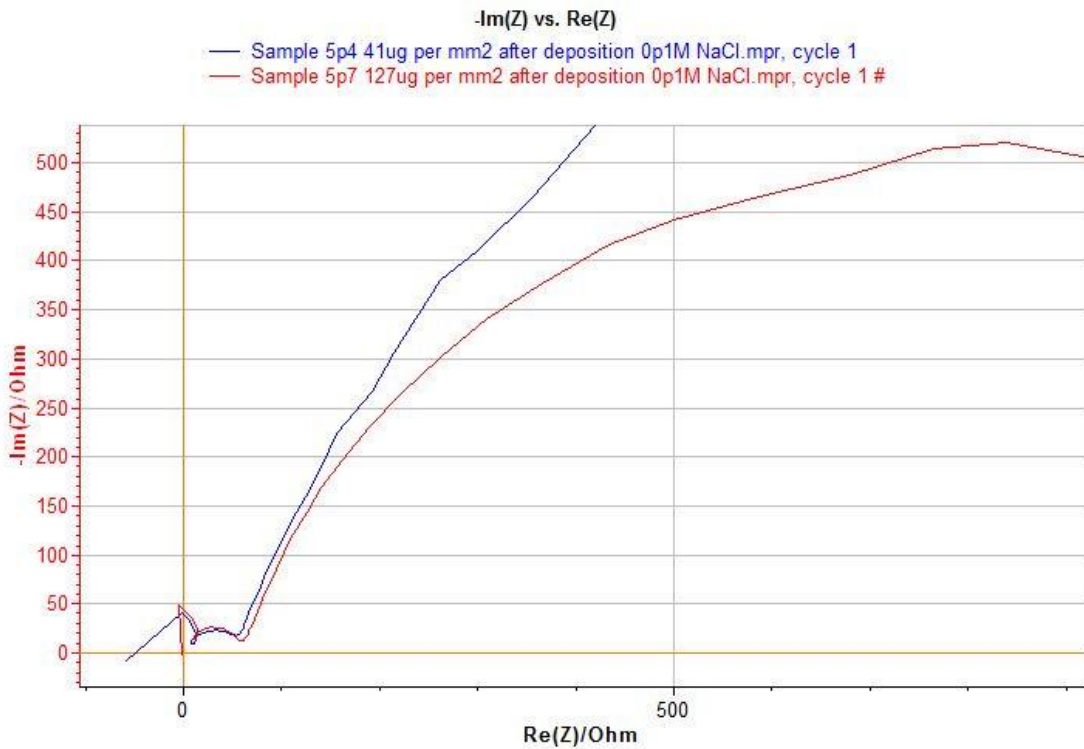— Sample 5p7 127ug per mm2 after deposition 0p1M NaCl.mpr, cycle 1 #

Figure 17: Zinc deposition in NaCl electrolyte. The thickness dependence can still be seen, and there are also second capacitive semicircles but they are much larger in this case. This is because the zeolite has a higher affinity for zinc than for sodium, so when the zinc is replaced with sodium in the zeolite, the impedance is higher [23].

26

Another observation to be made in figure 16 is that there is a second capacitive semicircle. This semicircle comes from a combination of the polarization resistance in the electrode and the double layer capacitance [22]. It can also be hinted in the NaCl case, but in this case it is much larger. The capacitance of this layer can be calculated as [22]:

$$C = \frac{1}{2\pi f_m R_p}$$

where f_m is the frequency at the top of the semicircle and R_p is the polarization resistance, which can be determined by the points where the semicircle intersects the x-axis. For the thick zeolite layer in the $ZnCl_2$ case, the frequency at the top of the semicircle is 100 Hz, and the semicircle intersects the x-axis at about 80 and 140 Ohm. This gives a polarization resistance of 60 Ohm, and a capacitance of 26.5 µF. In the NaCl case, the frequency is 1,5 Hz and the polarization resistance is 1500 Ohm, giving a capacitance of 70 µF. This difference is likely due to the fact that there are multiple ion species, and the zeolite has a higher affinity for zinc than for sodium [23]. When the electrolyte is $ZnCl_2$ there is an interchange between the zeolite and the electrolyte, but since it is the same type of ions, this exchange proceeds smoothly. When the electrolyte is NaCl, on the other hand, there is a dynamic ion exchange, giving rise to a higher impedance [23].

Futhermore, after each subsequent deposition in the $ZnCl_2$ case, the second semicircle shrinks, while no apparent trend can be seen in the NaCl case. This shrinkage of the second semicircle does not seem to depend on the time of deposition either. In the case shown in figure 16 above, the deposition was made by running -400 µA for 8 minutes, and the second semicircle was gone after three depositions (in all three cases). Therefore, an experiment with depositions of -400 µA for 1 minute was made (thickness 181 µg/mm^2), and the second semicircle was gone after the third deposition in this case as well. This indicates that perhaps

the phenomenon somehow only depends on the shifting of the potential, but it could also mean that the deposition is saturated already after 1 minute, and smaller times should be used to determine this. No further investigation was made, but this could perhaps play a role in battery conditioning.

A third observation to be made is that there are inductive semicircles in the low frequency region. In the pre-deposition graphs the lower frequencies were manifested with a straight line going diagonally upwards. This line is due to the so-called Warburg impedance and is related to diffusion. This impedance is small at high frequencies since diffusing reactants do not have to move very far, but at low frequencies they have to move further, increasing the Warburg impedance [24]. And since it only gives rise to a straight line, there was no reason to sweep the pre-deposition measurements further than 100 mHz. On the post-deposition graphs it is unclear which phenomenon the inductive semicircles come from, but it could be due to the non-steady state of the system at such low frequencies [23], [25].

5.2 Sol-gels

After the heat treatment the sol-gel had gelled well as can be seen in the picture to the left below. However, when dried, it shattered, as can be seen in the middle picture below. Freeze-drying was also tried but this did not work either, as can be seen in the right picture below.

Figure 19: Bulk sol-gel. Left: After gelation. Middle: After room temperature drying. Right: After freeze-drying. Neither drying method gave good results and attempts were more focused on thin-film sol-gel instead.

Therefore, more focus was put on the thin film recipes. Early on a fairly good layer of sol-gel was obtained on an electrode. A scratch was made in the surface and a microscope image of it can be seen in figure 20 below. The surface is fairly rough, but the scratch made is deeper, so the layer should be thick enough to cover the titanium entirely.
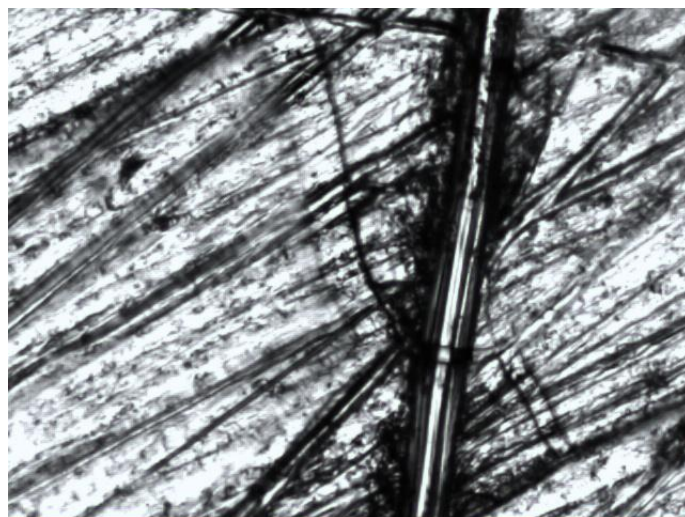
Figure 20: A scratch in a layer of thing-film sol-gel

Just to make sure, multiple dip electrodes were made as well. It had been reported [16] that in order to get a good surface for multiple dip, the electrode had to be dipped in a Na-containing solution (pH≥7), in between dips in the sol-gel. It was not specified what solution should be used, so in this case a NaCl solution (0.1M) was used, in which the electrodes were submerged for 3 minutes before the next layer of sol-gel was applied. At the same time, as a reference, multiple dip electrodes were made without dipping them in NaCl between sol-gel depositions. This gave one electrode with one dip, two electrodes with two dips (one with NaCl and one without), and two electrodes with three dips (same there). These were then cycled and compared to a blank electrode as a reference, and the result can be seen in table 2 below. The electrode with one dip did not perform well and the cycling experiment failed after just one deposition, but it can be seen that both double dip electrodes had the same efficiency, and for the triple dip electrodes there were an even higher efficiency in the case without the NaCl solution. There is also a clear trend that the more dips the better the efficiency, and also that ion pumping through the sol-gel works.

Table 2: Charge-discharge efficiencies of multiple-dip, thin-film sol-gel electrodes. The efficiency can be seen to increase but it is not guaranteed that the coating thickness is increased by the same amount per dip.

Electrode	Number of dips	NaCl-conditioned	Average efficiency (%)
ESG14:1	1	No	-
ESG14:3	2	Yes	44
ESG14:4	2	No	44
ESG14:2	3	Yes	63
ESG14:5	3	No	71
Blank	-	-	34

However, it should be stated that after the cycling, an attempt to scratch the sol-gel films were made to see if it was as good of a surface as in the microscope picture above, and in neither case was a clear scratch visible. This indicates that the coating seen in the microscope image above was thicker, even though it was only one dip. Therefore, it is not

necessarily the same thickness obtained from the same amount of dips, and the triple dip electrode without NaCl solution might just result in a thicker layer. At the same time the synthesis of electrodes were not straight forward, and a lot of the time they just became flaky or the sol-gel bunched together in grains on the surface, leaving patches of titanium bare. Furthermore, it was perceived to be easier to obtain a good surface when the electrodes were pre-laminated, so weighing the electrodes before and after the dipping in order to determine the thickness of the sol-gel would be very inconclusive. Also, a multitude of different attempts to obtain a good synthesis technique was tried. Varying the recipes, electrochemical polishing of the electrode, treating the electrodes with a base or an acid, trying different electrode materials such as gold mylar and silicon, different dip durations, pipetting the sol-gel onto the electrode instead of dip-coating it, a small amount of TEOS pipetted onto the electrode to provide extra building blocks. Nothing seemed to work, however.

It was therefore decided to try and synthesize sol-gel electrodes using an ammonia atmosphere, making it a base-catalyzed hydrolysis instead of an acid-catalyzed hydrolysis. This was done by mixing just the TEOS, DI water and ethanol, applying this mix onto the electrode and then putting the electrode in an ammonia atmosphere. Initially, it seemed fairly promising, and quite early a good electrode was made, as can be seen in the picture below

Figure 21: Sol-gel made form base-catalyzed hydrolysis in an ammonia atmosphere.

This electrode was cycled and the efficiency can be seen in the graph below. As can be seen, the average charge-discharge efficiency is 50%, but it is fairly low in the beginning (and the highest single efficiency is over 70%), and if the first three points would be omitted, the average efficiency would be 57%. The reason for the low efficiency in the beginning could be that there is an initial pumping of zinc ions into the film, but after the initial conditioning of the film the efficiency is clearly higher.
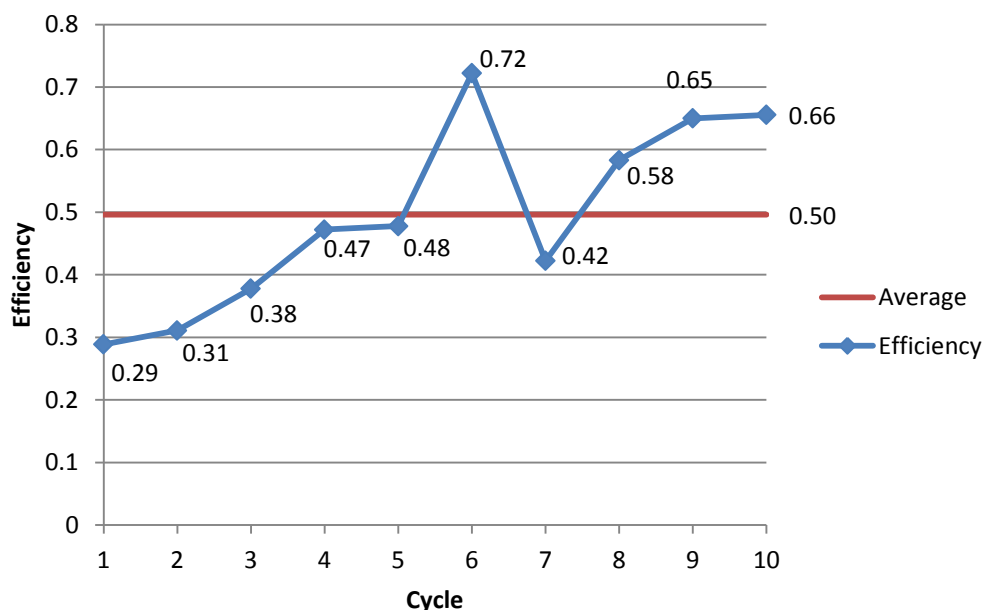
Figure 22: Efficiency of a base-catalyzed sample. The efficiency is raised compared to a blank sample, and there is a general rising trend as well.

This experiment implies that the ion pumping works with the base-catalyzed hydrolysis as well, but it would be interesting to try an experiment with more cycles to see if this high efficiency is sustained. However, there were problems with trying to recreate electrodes. Initially, they seemed stable, but when removed from the ammonia atmosphere they started cracking, as can be seen in figure 23 below.

Figure 23: Base-catalyzed sol-gel with cracks

Originally, the hypothesis was that the mix used had been allowed to set for too long. So even though no catalyst was present, there were still reactions going on in the solution, slowly forming a network causing the coating to crack upon drying. However, even with a fresh mix there were cracks coming up, and sometimes it seemed like the solution had just evaporated from the electrode. Therefore, experiments were made where the mix was refrigerated prior to application in order to give it more time to build the network before evaporating, but this did not, however, improve the coating. Another unsuccessful approach was to use a small vial of TEOS inserted in the ammonia atmosphere in order to saturate it with TEOS.

The experiments show that the concept with sol-gels as films over the electrodes work, both acid- and base-catalyzed hydrolysis, but the primary focus at the moment ought to be to find a good way to prepare the films on the electrodes. The amount of electrodes cycled and used in this report is only a very small fraction of the electrodes prepared. The base catalyzed electrodes had the aforementioned problems with cracking and evaporation, and most of the times the acid catalyzed sol-gel film turned flaky or bunched up and could not be used. The latter could, however, be due to the lack of proper dip coater, as these experiments were performed by simply submerging the electrodes for the appropriate time and then removing them by hand.

5.3 Silica gels

FTIR measurements were performed of the functionalized silica gel, and can be seen as the blue line in figure 24 below. This graph also contains the FTIR measurements of non-functionalized silica gel (red) and TMSPA (black) for reference. There are a number of interesting peaks apparent, and they are summarized in table 3 below [26]:

Table 3: FTIR peaks and their respective assignment [26]

Wavenumber (cm^{-1})	Assignment
3374	NH-stretching
3303	NH-stretching
2940	CH-stretching
2840	CH-stretching
1634	Overtone of NH-stretching
1600	NH_2-bending
1557	NH_2-bending
1489	CH_2-bending (in-plane)
1464	CH_2-bending (in-plane)
1333	C-O-stretching
1189	$C-H_2$-bending (out-of-plane)
1072	C-N-stretching
1052	Si-O-stretching
1027	Si-O-stretching

Since the silica gel itself is comprised solely of silica and oxygen with OH-terminals, it is natural that the red graph only has a wide OH peak around 3400 and a Si-O stretch peak at 1052.
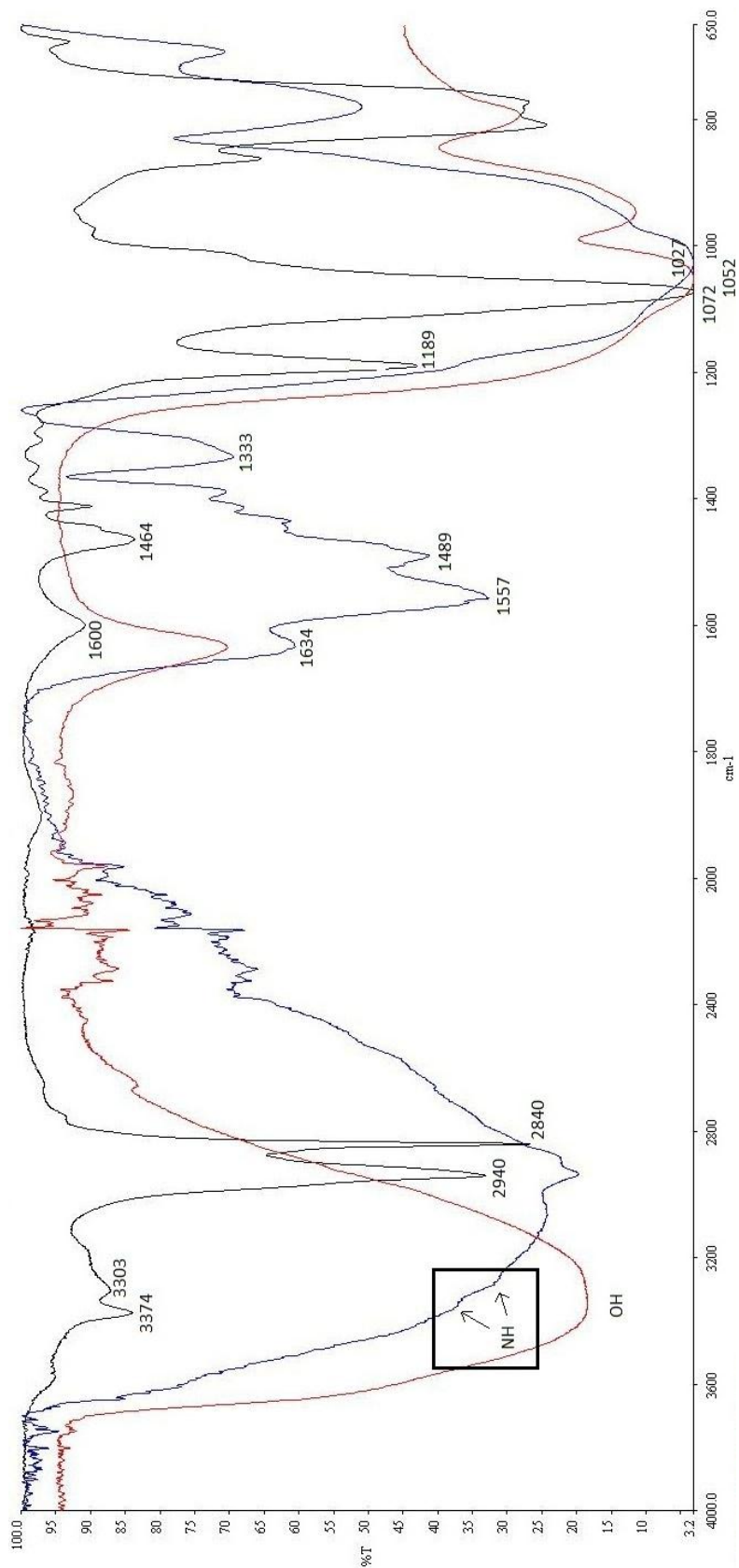
Figure 24: FTIR spectra of non-functionalized silica gel, functionalized silica gel, and the amine 3-Tremothoxysilane-propylamine. By comparing these graphs and their peaks it can be seen that the amine is incorporated into the silica gel, where especially the peaks around 3300 is important as those are the NH peaks (the amine that will give the molecular sieve property), and they can be seen as kinks in the functionalized silica gel.

The important peaks in the TMSPA are the NH_2-peaks at 3374 and 3303 cm^{-1} (stretch) and at 1600 cm^{-1} (bend), since these amine-peaks are the ones indicating that the chemical functionalization with amine groups was successful. Other signals proving the presence of the amino-propyl groups are the CH stretch peaks at 2940 and 2840 cm^{-1}, and the CH bend peak at 1464 cm^{-1}, but also the CO stretch peak at 1189 cm^{-1} and the CN bend peak at 1072 cm^{-1}. Furthermore, the peaks at 1333 and 1557 cm^{-1} are very important since they are only apparent in the functionalized silica gel graph. The emergence of new peaks is a proof that the two substances are chemically bound and does not merely co-exist.

For the functionalized silica gel graph, the NH_2 stretching peaks can be seen as kinks on the OH peak, indicating that the TMSPA has been incorporated in the silica network. This incorporation is further proved by the other peaks apparent in the graph for the functionalized silica gel, and the functionalization is therefore successful.

For the making of the films, the binder polystyrene was first used as that was what was used for the zeolites. There were more troubles with getting a good film on the electrodes with this mix than with the zeolites, with a lot of cracks showing up. Some films were cycled though, and the best result for these films can be seen in the graph below:
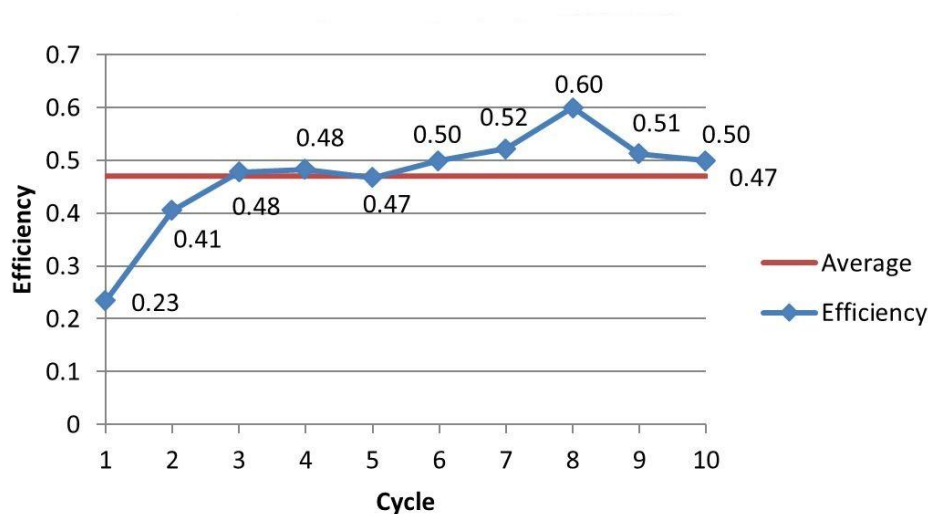

Figure 25: Efficiency of silica gel film mixed with PS binder.

The average efficiency was thus 47%, which is somewhat higher than the efficiency of around 30% for the blank samples. However, other samples held efficiencies of 36, 38 and 41% respectively. This is believed to be due to the hydrophobicity of the PS while the silica gel is hydrophilic, and they should therefore not mix very well.

Therefore, other non-hydrophobic binders were tried instead, namely PVA and PC. The film created with PVA broke upon electrode lamination. The film created with PC was also prone to cracking during synthesis, and it was hard to get a good film. The only PC film cycled had an average efficiency of 22%, which is even lower than for the blank samples.

6. Conclusion and perspectives

In the zeolite case, the impedance was found to depend on the thickness of the zeolite layers. However, if a lot of charge is to be deposited or if an electrolyte without zinc is used, a balance of thickness has to be made in order to be able to host enough zinc to function properly. Furthermore, some interesting phenomena were found that could be investigated further, such as the time dependence of the polarization resistance.

The sol-gel experiments showed proof of concept, both for acid and base catalyzed hydrolysis, proving that the ion pumping works and that the efficiency could be raised compared to blank samples. It is possible that the efficiency can be further improved by functionalizing these films (as no good electrodes with functionalized sol-gel were obtained in this thesis). Furthermore, as it is now, some of the energy loss could be due to parasitic reactions that can be avoided by changing the pH of the electrolyte or using different currents. These are optimization experiments, however, and this report is content with proof of concept. Further experiments should primarily focus on finding a good method of preparation, as the amount of electrodes cycled in this thesis was far lower than the amount of electrodes that were prepared.

As in the sol-gel case, an increase of efficiency was obtained by the silica gel as compared to a blank electrode, so this concept works as well. It was also proven that the functionalization works for the silica gel, which is promising for the sol-gel case. However, the increased efficiency in the silica gel case was rather small, but this was likely due to the fact that no good binder was found, and the binder issue is what further experiments ought to focus on.

References

1.   Bard and Faulkner, *Electrochemical Methods, Fundamentals and Applications*. 2nd ed. 2001, United States of America: John Wiley and sons inc.

2.   *Gamry Instruments Application Note: Basics of Electrochemical Impedance Spectroscopy*: http://www.gamry.com/assets/Application-Notes/Basics-of-EIS.pdf.

3.   *European Commission Directorate-General for Energy: The future role and challenges of Energy Storage*, 2013 [Accessed 2013-03-07], Available from: http://ec.europa.eu/energy/infrastructure/doc/energy-storage/2013/energy_storage.pdf.

4.   Cairns, E.J., *Batteries, Overview*, in *Encyclopedia of Energy*, J.C. Editor-in-Chief: Cutler, Editor. 2004, Elsevier: New York. p. 117-126.

5.   Nationalencyclopedin. [Accessed 2013-03-07]; Available from: http://www.ne.se/lang/batteri/124967.

6.   Dell, R.M., *Batteries: fifty years of materials development.* Solid State Ionics, 2000. **134**(1–2): p. 139-158.

7.   Arai, H. and M. Hayashi, *SECONDARY BATTERIES – METAL-AIR SYSTEMS | Overview (Secondary and Primary)*, in *Encyclopedia of Electrochemical Power Sources*, G. Editor-in-Chief: Jürgen, Editor. 2009, Elsevier: Amsterdam. p. 347-355.

8.   Haas, O. and J. Van Wesemael, *SECONDARY BATTERIES – METAL-AIR SYSTEMS | Zinc–Air: Electrical Recharge*, in *Encyclopedia of Electrochemical Power Sources*, G. Editor-in-Chief: Jürgen, Editor. 2009, Elsevier: Amsterdam. p. 384-392.

9.   Harting, K., U. Kunz, and T. Turek, *Zinc-air batteries: Prospects and challenges for future improvement.* Zeitschrift fur Physikalische Chemie, 2012. **226**(2): p. 151-166.

10.   Matthias Hilder, Monash University, personal communication.

11.   Nationalencyclopedin. [Accessed 2012-11-10]; Available from: http://www.ne.se/lang/zeoliter.

12.   Hench, L.L. and J.K. West, *The Sol-Gel process.* Chemical Reviews, 1990. **90**(1): p. 33-72.

13.   Siouffi, A.M., *Silica gel-based monoliths prepared by the sol–gel method: facts and figures.* Journal of Chromatography A, 2003. **1000**(1–2): p. 801-818.

14.   Nationalencyclopedin. [Accessed 2013-04-02]; Available from: http://www.ne.se/lang/kiselgel.

15. Luther-Davies, B., M. Samoc, and M. Woodruff, *Comparison of the Linear and Nonlinear Optical Properties of Poly(p-phenylenevinylene)/Sol-Gel Composites Derived from Tetramethoxysilane and Methyltrimethoxysilane.* Chemistry of Materials, 1996. **8**(11): p. 2586-2594.

16. Radin, S. and P. Ducheyne, *Controlled release of vancomycin from thin sol-gel films on titanium alloy fracture plate material.* Biomaterials, 2007. **28**(9): p. 1721-1729.

17. Hamdy, A.S., D.P. Butt, and A.A. Ismail, *Electrochemical impedance studies of sol-gel based ceramic coatings systems in 3.5% NaCl solution.* Electrochimica Acta, 2007. **52**(9): p. 3310-3316.

18. Nationalencyclopedin. [Accessed 2013-02-05]; Available from: http://www.ne.se/aminer.

19. Berthomieu, C. and R. Hienerwadel, *Fourier transform infrared (FTIR) spectroscopy.* Photosynthesis Research, 2009. **101**(2-3): p. 157-170.

20. Nationalencyklopedin. [Accessed 2013-03-01]; Available from: http://www.ne.se/infrarödspektroskopi.

21. Griffiths, P.R. and J.A.d. Haseth, *Fourier Transform Infrared Spectroscopy*. 2nd ed. 2007, Hoboken, New Jersey: John Wiley & sons.

22. Foyet, A., A. Hauser, and W. Schäfer, *Template electrochemical deposition and characterization of zinc–nickel alloy nanomaterial.* Journal of Electroanalytical Chemistry, 2007. **604**(2): p. 137-143.

23. Bjorn Winther-Jensen, Monash University, personal communication.

24. Vedalakshmi, R., et al., *Determination of diffusion coefficient of chloride in concrete using Warburg diffusion coefficient.* Corrosion Science, 2009. **51**(6): p. 1299-1307.

25. Ganne, F., et al., *Impedance spectroscopy and modelling of zinc deposition in chloride electrolyte containing a commercial additive.* Journal of Applied Electrochemistry, 2000. **30**(6): p. 665-673.

26. Silverstein, Bassler, and Morrill, *Spectrometric Identification of Organic Compounds*. 5 ed. 1991: John Wiley & Sons, Inc.